Anti-Windup Compensation for Quadrotor Trajectory Tracking With External Disturbances

Majid Shahbazzadeh and Christopher M. Richards, *Member, IEEE*

***Abstract*—This letter considers the problem of trajectory tracking for quadrotors operating in wind conditions that result in propeller thrust saturation. To address this problem, an anti-windup compensator (AWC) is developed to reduce the tracking performance degradation and destabilizing effects from thrust saturation. Relationships are derived showing how the tracking error and AWC states are influenced by the wind disturbance and saturation, and how the influences depend on the controller and AWC gains. As a result, these gains can be tuned to achieve desired performance levels. Simulation results are presented to validate the effectiveness of the proposed method.**

***Index Terms*—Quadrotors, tracking, anti-windup.**

I. Introduction

QUADROTOR uncrewed aerial vehicles (UAVs) offer several advantages, such as vertical takeoff and landing and cost-effectiveness [1], [2], [3]. These attributes have led to their use in a wide range of applications, including rescue missions, mapping, surveillance, and inspections [4], [5], [6], [7]. Achieving stable hovering and safe flight is crucial for these UAVs to effectively perform their intended functions [8].

A quadrotor is an under-actuated nonlinear system, characterized by four individual rotors that control highly coupled states [9], [10]. The primary challenge in the trajectory tracking problem is the design of a controller for attitude control since the vehicle's under-actuated nature requires that position tracking be managed through the control of its rotational dynamics [10]. Likewise, wind disturbances pose a significant challenge to the stability and control of these systems [11], [12]. When subjected to strong winds, the quadrotor may experience deviations from the desired trajectory. To counteract such disturbances, the control system demands high propeller speeds. However, if wind forces exceed the propellers' capability to counteract the wind, the controllers propeller speed demand might surpass the motors' maximum achievable speed limits, leading to saturation. Saturation hinders the propellers from generating adequate thrust, and can cause instability in the closed-loop system.

Received 16 September 2024; revised 12 November 2024; accepted 2 December 2024. Date of publication 11 December 2024; date of current version 26 December 2024. This work was supported by the National Science Foundation under Award TI-2219008. Recommended by Senior Editor S. Tarbouriech. *(Corresponding author: Christopher M. Richards.)*

The authors are with the Department of Mechanical Engineering, University of Louisville, Louisville, KY 40292 USA (e-mail: majid.shahbazzadeh@louisville.edu; chris.richards@louisville.edu).

Digital Object Identifier 10.1109/LCSYS.2024.3516635

The actuator saturation problem has attracted considerable attention over the past few decades, resulting in the development of various methods to address it in control systems. One of these methods is to ensure that the control signals remain within the specified saturation bounds. For example, the saturation avoidance problem has been addressed in [13], [14] using linear matrix inequalities. However, approaches such as these may be conservative in some problems, leading to control signals that operate significantly below their saturation levels. Moreover, external disturbances may cause control signal saturation that is unavoidable.

Anti-windup compensation (AWC) is a common augmentation to control systems that can effectively handle control signal saturation [15], [16], [17], [18]. For managing disturbances, an anti-windup framework has been proposed for stable plants [19]. Specifically for quadrotors, whose dynamics are inherently unstable, an anti-windup scheme is presented for input-coupled double integrator systems [20], which is applicable when quadrotor dynamics are linearized about hover. In addition, an architecture combining static and dynamic AWC has been presented [21]. Although other studies have also focused on the design of AWC for quadrotors [22], [23], [24], to the best of our knowledge, consideration of disturbance in AWC design for quadrotors has not been *directly* addressed. This issue motivates our paper. While AWC is one effective solution, other methods for mitigating the effects of saturation also exist. However, the focus here is exclusively on AWC, highlighting its advantages in stabilizing the quadrotor under wind disturbances while achieving desired performance levels.

In this letter, the focused application of the AWC is for trajectory tracking control. To reduce the impact of saturation and disturbance on the tracking error, significant upper bounds are analytically obtained, which allow for the tuning of the controller and AWC gains to achieve the desired performance. Simulation results are presented to illustrate the effectiveness and validity of the proposed method.

II. Problem Formulation

The saturation and deadzone functions are defined as

$$\mathrm{sat}_{\underline{u}_i}^{\overline{u}_i}(u_i) = \begin{cases} \overline{u}_i & \overline{u}_i < u_i \\ u_i & \underline{u}_i \le u_i \le \overline{u}_i \\ \underline{u}_i & u_i < \underline{u}_i \end{cases} \tag{1}$$

$$\mathrm{Dz}_{\underline{u}_i}^{\overline{u}_i}(u) = u_i - \mathrm{sat}_{\underline{u}_i}^{\overline{u}_i}(u_i), \tag{2}$$

where $\mathrm{sat}_{\underline{u}}^{\overline{u}}(u) = [\mathrm{sat}_{\underline{u}_1}^{\overline{u}_1}(u_1), \ldots, \mathrm{sat}_{\underline{u}_m}^{\overline{u}_m}(u_m)]'$ and $\mathrm{Dz}_{\underline{u}}^{\overline{u}}(u) = [\mathrm{Dz}_{\underline{u}_1}^{\overline{u}_1}(u_1), \ldots, \mathrm{Dz}_{\underline{u}_m}^{\overline{u}_m}(u_m)]'$.

The translational dynamics of a quadrotor with constrained thrust (T) in the inertial frame can be expressed as

$$m\dot{u} = -\left(\mathrm{c}_\phi \mathrm{s}_\theta \mathrm{c}_\psi + \mathrm{s}_\phi \mathrm{s}_\psi\right)\mathrm{sat}_{\underline{T}}^{\overline{T}}(T) + d_u, \tag{3}$$

$$m\dot{v} = -\left(\mathrm{c}_\phi \mathrm{s}_\theta \mathrm{s}_\psi - \mathrm{s}_\phi \mathrm{c}_\psi\right)\mathrm{sat}_{\underline{T}}^{\overline{T}}(T) + d_v, \tag{4}$$

$$m\dot{w} = mg - \mathrm{c}_\phi \mathrm{c}_\theta \mathrm{sat}_{\underline{T}}^{\overline{T}}(T) + d_w, \tag{5}$$

where T is the total propeller thrust perpendicular to the vehicle's plane, m is the mass of the vehicle, d_u, d_v, d_w are the external disturbances, $[u, v, w] = [\dot{x}, \dot{y}, \dot{z}]$, and x, y, and z are the position coordinates in the inertial frame.

The angular velocity dynamics with constrained body torques (τ) in the body frame can be described as

$$J\dot{\omega} = -\omega \times J\omega + \mathrm{sat}_{\underline{\tau}}^{\overline{\tau}}(\tau) + d_\Gamma, \tag{6}$$

where $\tau = [\tau_1, \tau_2, \tau_3]'$ is the control torque vector, $\omega = [\omega_1, \omega_2, \omega_3]'$ is the angular velocity vector, $d_\Gamma = [d_{\Gamma_1}, d_{\Gamma_2}, d_{\Gamma_3}]'$ is the external disturbance vector, and $J = \mathrm{diag}\{J_1, J_2, J_3\}$ is the inertia matrix.

The vector ω can be expressed as $\omega = Q\dot{\Gamma}$, where

$$Q = \begin{bmatrix} 1 & 0 & -\mathrm{s}_\theta \\ 0 & \mathrm{c}_\phi & \mathrm{s}_\phi \mathrm{c}_\theta \\ 0 & -\mathrm{s}_\phi & \mathrm{c}_\phi \mathrm{c}_\theta \end{bmatrix}, \quad \Gamma = \begin{bmatrix} \phi \\ \theta \\ \psi \end{bmatrix}, \tag{7}$$

$\mathrm{c}_\delta = \cos\delta$, $\mathrm{s}_\delta = \sin\delta$, and ϕ, θ, and ψ are roll, pitch, and yaw Euler angles, respectively.

Linearization of the quadrotor dynamics around the hover operating point and utilizing (2) results in

$$\begin{bmatrix} m\dot{w} \\ J_i\dot{\Gamma}_i \end{bmatrix} = \begin{bmatrix} mg - T + \mathrm{Dz}_{\underline{T}}^{\overline{T}}(T) + d_w \\ \tau_i - \mathrm{Dz}_{\underline{\tau}_i}^{\overline{\tau}_i}(\tau_i) + d_{\Gamma_i} \end{bmatrix}, \quad i = 1, 2, 3 \tag{8}$$

Assumption 1: The external disturbances d_u, d_v, d_w and d_{Γ_i} are assumed to be due to wind gusts. Therefore, they are finite-duration bounded signals and belong to the $\mathcal{L}_2$ space.

Remark 1: In the theoretical results, the control torque τ and control thrust T are the signals that are constrained by the saturation function. However, for a quadrotor, the speeds of each propeller are what are physically limited. Therefore, in order to implement the proposed method, the following process is executed. First, the propeller speed commands are obtained from the thrust and torque control signals as follows:

$$\underbrace{\begin{bmatrix} \varpi_1^2 \\ \varpi_2^2 \\ \varpi_3^2 \\ \varpi_4^2 \end{bmatrix}}_{\tilde{\varpi}} = \underbrace{\begin{bmatrix} \frac{1}{4k} & \frac{1}{4kl} & \frac{1}{4kl} & \frac{1}{4b} \\ \frac{1}{4k} & \frac{-1}{4kl} & \frac{1}{4kl} & \frac{-1}{4b} \\ \frac{1}{4k} & \frac{-1}{4kl} & \frac{-1}{4kl} & \frac{1}{4b} \\ \frac{1}{4k} & \frac{1}{4kl} & \frac{-1}{4kl} & \frac{-1}{4b} \end{bmatrix}}_{\Pi} \begin{bmatrix} T \\ \tau_1 \\ \tau_2 \\ \tau_3 \end{bmatrix}, \tag{9}$$

where l, k, and b are the thrust moment arm, the propeller thrust constant, and the propeller drag constant, respectively. Next, the propeller speed commands are constrained by $\mathrm{sat}_0^{\overline{\varpi}^2}(\varpi_i^2) = \min(\max(\varpi_i^2, 0), \overline{\varpi}^2)$, $i = 1, \ldots, 4$. Then, the saturated control thrust and torques are obtained from

$$\begin{bmatrix} \mathrm{sat}_{\underline{T}}^{\overline{T}}(T) \\ \mathrm{sat}_{\underline{\tau}_1}^{\overline{\tau}_1}(\tau_1) \\ \mathrm{sat}_{\underline{\tau}_2}^{\overline{\tau}_2}(\tau_2) \\ \mathrm{sat}_{\underline{\tau}_3}^{\overline{\tau}_3}(\tau_3) \end{bmatrix} = \underbrace{\begin{bmatrix} k & k & k & k \\ kl & -kl & -kl & kl \\ kl & kl & -kl & -kl \\ b & -b & b & -b \end{bmatrix}}_{\Pi^{-1}} \begin{bmatrix} \mathrm{sat}_0^{\overline{\varpi}^2}(\varpi_1^2) \\ \mathrm{sat}_0^{\overline{\varpi}^2}(\varpi_2^2) \\ \mathrm{sat}_0^{\overline{\varpi}^2}(\varpi_3^2) \\ \mathrm{sat}_0^{\overline{\varpi}^2}(\varpi_4^2) \end{bmatrix} \tag{10}$$

Equations (9) and (10) are used in Section V for simulation.

III. Main Results

In this section, two theorems, a corollary, and a lemma are provided for general first-order, stable, single-input, single-output systems, which are later used to derive results specifically for the quadrotor tracking problem with constrained torque and thrust signals.

Theorem 1: Consider the following system:

$$\eta\dot{x}_p = -k_p x_p + \mathrm{Dz}_{\underline{u}_p}^{\overline{u}_p}(u_p)/\mu, \tag{11}$$

where $\overline{u}_p > 0$ and $\underline{u}_p < 0$ are upper and lower saturation bounds, respectively. Then, for $u_p = \mu k_p x_p, \mu \neq 0$, and $\eta > 0.$, it can be concluded that $x_p \to 0$ for any $k_p > 0$.

Proof of Theorem 1: Consider the Lyapunov function:

$$V(x_p) = \frac{k_p \eta}{2} x_p^2. \tag{12}$$

The time-derivative of (12) along the solutions of (11) yields:

$$\dot{V}(x_p) = k_p \eta x_p \dot{x}_p = -k_p^2 x_p^2 + \frac{k_p}{\mu} x_p \mathrm{Dz}_{\underline{u}_p}^{\overline{u}_p}(u_p). \tag{13}$$

In addition, the following sector condition is always satisfied:

$$\mathrm{Dz}_{\underline{u}_p}^{\overline{u}_p}(u_p)\omega\left(u_p - \mathrm{Dz}_{\underline{u}_p}^{\overline{u}_p}(u_p)\right) \geq 0, \quad \omega > 0, \tag{14}$$

which, for $\omega = 1/\mu^2$, leads to

$$\frac{k_p}{\mu} x_p \mathrm{Dz}_{\underline{u}_p}^{\overline{u}_p}(u_p) - \left(\frac{\mathrm{Dz}_{\underline{u}_p}^{\overline{u}_p}(u_p)}{\mu}\right)^2 \geq 0. \tag{15}$$

Adding (15) to the right-hand side of (13) results in

$$\dot{V}(x_p) \leq -k_p^2 x_p^2 + \frac{2k_p}{\mu} x_p \mathrm{Dz}_{\underline{u}_p}^{\overline{u}_p}(u_p) - \left(\frac{\mathrm{Dz}_{\underline{u}_p}^{\overline{u}_p}(u_p)}{\mu}\right)^2, \tag{16}$$

which, with the use of (2), leads to

$$\dot{V}(x_p) \leq -\left(\frac{\mathrm{sat}_{\underline{u}_p}^{\overline{u}_p}(u_p)}{\mu}\right)^2. \tag{17}$$

Only if $x_p = 0$, we have $\mathrm{sat}_{\underline{u}_p}^{\overline{u}_p}(u_p) = 0$. Therefore, $\dot{V}(x_p) < 0$, $\forall x_p \neq 0$, implying $x_p \to 0$. ■

Theorem 2: Consider the following system:

$$\sigma\dot{x}_q = -k_q x_q + v, \tag{18}$$

where $x_q(0) = 0, \sigma > 0$, and $v \in \mathcal{L}_2$. For any $k_q > 1$:

$$\|x_q\|/\|v\| \leq \gamma, \tag{19}$$

where

$$1/\left(2\sqrt{k_q - 1}\right) \leq \gamma. \tag{20}$$

Proof of Theorem 2: Consider the Lyapunov function:

$$V_q = \frac{1}{2}\sigma x_q^2, \tag{21}$$

and the following performance index:

$$\mathcal{J} = \int_0^\infty \left(x_q^2 - \gamma^2 v^2\right)\mathrm{d}t. \tag{22}$$

Note that if $\mathcal{J} \leq 0$, then condition (19) is satisfied.

For zero initial condition,

$$\mathcal{J} \leq \mathcal{J} + \underbrace{V_q\big(x_q(\infty)\big)}_{\geq 0} - \underbrace{V_q\big(x_q(0)\big)}_{=0}. \tag{23}$$

The right-hand side of (23) can be rewritten as

$$\int_0^\infty \Big(\dot{V}_q(x_q) + x_q^2 - \gamma^2 \nu^2\Big) \mathrm{d}t. \tag{24}$$

Therefore, $\mathcal{J} \leq 0$ is satisfied if

$$\dot{V}_q\big(x_q\big) + x_q^2 - \gamma^2 \nu^2 \leq 0. \tag{25}$$

The above inequality can be rewritten as

$$\left(1 - k_q + \frac{1}{4\gamma^2}\right) x_q^2 - \left(\frac{1}{2\gamma} x_q - \gamma \nu\right)^2 \leq 0. \tag{26}$$

Inequality (26) is always satisfied if

$$1 - k_q + 1/\Big(4\gamma^2\Big) \leq 0, \tag{27}$$

which, for $k_q > 1$, implies (20). Therefore, the lower bound on γ is $\gamma_{\min} = 1/(2\sqrt{k_q - 1})$. ■

Remark 2: According to (20), one can obtain

$$k_q \geq 1 + 1/\Big(4\gamma^2\Big). \tag{28}$$

Therefore, gain k_q can be determined by setting γ.

Corollary 1: Consider the dynamics (18). If ν is a finite-duration bounded signal, it can be concluded that $x_q \to 0$.

Proof of Corollary 1: Suppose that there is a finite time $\bar{t}$ such that $\nu = 0$ for $t \geq \bar{t}$. It follows from (18) that

$$\dot{x}_q = -\big(k_q/\sigma\big) x_q, \quad t \geq \bar{t}. \tag{29}$$

Since $k_q/\sigma > 0$, then $x_q \to 0$. ■

Lemma 1: Let r, r_d, r_r, and r_e be scalar signals. If $r_e = r - r_d - r_a$, the following inequality holds:

$$\|r - r_d\| \leq \sqrt{2\|r_e\|^2 + 2\|r_a\|^2}. \tag{30}$$

Proof of Lemma 1: We have

$$r - r_d = r_e + r_a. \tag{31}$$

In addition, it follows from $(r_e - r_a)^2 \geq 0$ that $2r_e r_a \leq r_e^2 + r_a^2$. Therefore, one can write

$$(r_e + r_a)^2 = r_e^2 + r_a^2 + 2r_e r_a \leq 2\Big(r_e^2 + r_a^2\Big). \tag{32}$$

From (31) and (32), we have

$$(r - r_d)^2 = (r_e + r_a)^2 \leq 2\Big(r_e^2 + r_a^2\Big). \tag{33}$$

Integrating from 0 to ∞ and square rooting leads to (30). ■

Lemma 2: The following holds for any vectors a and b [25]:

$$\mathrm{Dz}_{\underline{u}}^{\overline{u}}(a + b) = \mathrm{Dz}_{\underline{u}-a}^{\overline{u}-a}(b). \tag{34}$$

IV. Quadrotor Tracking Problem

A. Control and AWC Design

Define $[u_d, v_d, w_d] = [\dot{x}_d, \dot{y}_d, \dot{z}_d]$, where x_d, y_d, and z_d are the desired position coordinates in the inertial frame. In addition, define $\Gamma_d = [\Gamma_{d_1}, \Gamma_{d_2}, \Gamma_{d_3}]' = [\dot{\phi}_d, \dot{\theta}_d, \dot{\psi}_d]'$, where ϕ_d, θ_d, and ψ_d are the desired roll, pitch, and yaw angles.

The control torques and thrust are constructed as

$$T = m(g - \dot{w}_d) + k_w w_e + k_a w_a, \tag{35}$$

$$\tau_i = J_i \dot{\Gamma}_{d_i} - K_{\Gamma_i} \Gamma_{e_i} - K_{a_i} \Gamma_{a_i}, \tag{36}$$

where k_w, K_{Γ_i} are control gains, k_a, K_{a_i} are AWC gains, $w_e = w - w_d - w_a$, and $\Gamma_{e_i} = \Gamma_i - \Gamma_{d_i} - \Gamma_{a_i}$. In addition, w_a and Γ_{a_i} are the AWC states of the following AWC dynamics:

$$m\dot{w}_a = -k_a w_a + \mathrm{Dz}_{\underline{T}}^{\overline{T}}(T), \tag{37}$$

$$J_i \dot{\Gamma}_{a_i} = -K_{a_i} \Gamma_{a_i} - \mathrm{Dz}_{\underline{\tau}_i}^{\overline{\tau}_i}(\tau_i). \tag{38}$$

Assumption 2: For tracking the desired signal, the following conditions should be satisfied:

$$\underline{T} < m(g - \dot{w}_d) < \overline{T}, \qquad \underline{\tau}_i < J_i \dot{\Gamma}_{d_i} < \overline{\tau}_i. \tag{39}$$

These are reasonable requirements, as (39) states that the thrust and torques required to track the desired vertical translational velocity and angular velocities should not exceed the available thrust and torques that the quadrotor can provide.

By inserting (35) and (36) into (8), one obtains

$$m(\dot{w} - \dot{w}_d) = -k_w w_e - k_a w_a + \mathrm{Dz}_{\underline{T}}^{\overline{T}}(T) + d_w, \tag{40}$$

$$J_i\big(\dot{\Gamma}_i - \dot{\Gamma}_{d_i}\big) = -K_{\Gamma_i} \Gamma_{e_i} - K_{a_i} \Gamma_{a_i} - \mathrm{Dz}_{\underline{\tau}_i}^{\overline{\tau}_i}(\tau_i) + d_{\Gamma_i}. \tag{41}$$

Subtracting (37) and (38) from (40) and (41) results in the error dynamics

$$m\dot{w}_e = -k_w w_e + d_w, \;\; J_i \dot{\Gamma}_{e_i} = -K_{\Gamma_i} \Gamma_{e_i} + d_{\Gamma_i}. \tag{42}$$

Corollary 2: Consider the error dynamics (42) and Assumption 1. Then $w_e \to 0, \Gamma_{e_i} \to 0$, and the following conditions are satisfied:

$$\|w_e\|/\|d_w\| \leq \gamma_w, \tag{43}$$

$$\|\Gamma_{e_i}\|/\|d_{\Gamma_i}\| \leq \gamma_{\Gamma_i}, \quad i = 1, 2, 3. \tag{44}$$

where $1/(2\sqrt{k_w - 1}) \leq \gamma_w$ and $1/(2\sqrt{K_{\Gamma_i} - 1}) \leq \gamma_{\Gamma_i}$.

Proof of Corollary 2: It follows from Theorem 2 that by considering $\sigma = m, x_q = w_e, k_q = k_w, \nu = d_w$, and $\sigma = J_i, x_q = \Gamma_{e_i}, k_q = K_{\Gamma_i}, \nu = d_{\Gamma_i}$ in (18) leads to (43) and (44). Also, from Corollary 1: $w_e \to 0$ and $\Gamma_{e_i} \to 0$. ■

Corollary 3: Consider the AWC dynamics (37) and (38) and Assumption 2. It can be concluded that $w_a \to 0, \Gamma_{a_i} \to 0$, and the following conditions are satisfied:

$$\|w_a\|/\|\mathrm{Dz}_{\underline{T}}^{\overline{T}}(T)\| \leq \gamma_a, \tag{45}$$

$$\|\Gamma_{a_i}\|/\|\mathrm{Dz}_{\underline{\tau}_i}^{\overline{\tau}_i}(\tau_i)\| \leq \gamma_{A_i}, \quad i = 1, 2, 3, \tag{46}$$

where $1/(2\sqrt{k_a - 1}) \leq \gamma_a$ and $1/(2\sqrt{K_{a_i} - 1}) \leq \gamma_{A_i}$.

Proof of Corollary 3: Segregating the control inputs as

$$T = \underbrace{m(g - \dot{w}_d) + k_w w_e}_{T_\alpha} + \underbrace{k_a w_a}_{T_\beta}, \tag{47}$$

$$\tau_i = \underbrace{J\dot{\Gamma}_{d_i} - K_{\Gamma_i} \Gamma_{e_i}}_{\tau_{\alpha_i}} \underbrace{-K_{a_i} \Gamma_{a_i}}_{\tau_{\beta_i}}. \tag{48}$$

From Lemma 2, we have

$$\mathrm{Dz}^{\overline{T}}_{\underline{T}}(T) = \mathrm{Dz}^{\overline{T}_n}_{\underline{T}_n}(T_\beta), \quad \mathrm{Dz}^{\overline{\tau}_i}_{\underline{\tau}_i}(\tau_i) = \mathrm{Dz}^{\overline{\tau}_{n_i}}_{\underline{\tau}_{n_i}}(\tau_{\beta_i}), \tag{49}$$

where $\overline{T}_n = \overline{T} - T_\alpha$, $\underline{T}_n = \underline{T} - T_\alpha$, $\overline{\tau}_{n_i} = \overline{\tau}_i - \tau_{\alpha_i}$, $\underline{\tau}_{n_i} = \underline{\tau}_i - \tau_{\alpha_i}$.

Substituting (49) into (37) and (38) results in

$$\begin{aligned} m\dot{w}_a &= -k_a w_a + \mathrm{Dz}^{\overline{T}_n}_{\underline{T}_n}(k_a w_a), \\ J_i \dot{\Gamma}_{a_i} &= -K_{a_i}\Gamma_{a_i} - \mathrm{Dz}^{\overline{\tau}_{n_i}}_{\underline{\tau}_{n_i}}(-K_{a_i}\Gamma_{a_i}). \end{aligned} \tag{50}$$

It follows from Corollary 2 that $w_e \to 0$ and $\Gamma_{e_i} \to 0$ consequently $T_\alpha \to m(g - \dot{w}_d)$ and $\tau_{\alpha_i} \to J_i \dot{\Gamma}_{d_i}$. Thus, from Assumption 2, there exists a finite time t_1 such that

$$\underline{T} < T_\alpha < \overline{T}, \quad \underline{\tau}_i < \tau_{\alpha_i} < \overline{\tau}_i, \quad \forall t \geq t_1, \tag{51}$$

leading to $\underline{T}_n < 0, \overline{T}_n > 0$, and $\underline{\tau}_{n_i} < 0, \overline{\tau}_{n_i} > 0, \ \forall t \geq t_1$.

From Theorem 1, by considering $\eta = m$, $k_p = k_a$, $\mu = 1, \overline{u}_p = \overline{T}_n, \underline{u}_p = \underline{T}_n, x_p = w_a$, and $\eta = J_i, k_p = K_{a_i}, \mu = -1, \overline{u}_p = \overline{\tau}_{n_i}, \underline{u}_p = \underline{\tau}_{n_i}, x_p = \Gamma_{a_i}$ in (11), it can be concluded that $w_a \to 0$ and $\Gamma_{a_i} \to 0$. In addition, since $w_e \to 0, \Gamma_{e_i} \to 0$, it can be deduced that $\mathrm{Dz}^{\overline{T}}_{\underline{T}}(T) \in \mathcal{L}_2$ and $\mathrm{Dz}^{\overline{\tau}_i}_{\underline{\tau}_i}(\tau_i) \in \mathcal{L}_2$.

It follows from Theorem 2 that comparison of the AWC dynamics (37) and (38) and the dynamics (18) through the following substitution: $\sigma = m, k_q = k_a, x_q = w_a, \nu = \mathrm{Dz}^{\overline{T}}_{\underline{T}}(T)$, and $\sigma = J_i, k_q = K_{a_i}, x_q = \Gamma_{a_i}, \nu = -\mathrm{Dz}^{\overline{\tau}_i}_{\underline{\tau}_i}(\tau_i)$ leads to the proof of (45) and (46), respectively. ∎

Corollary 4: Consider $w_e = w - w_d - w_a, \Gamma_{e_i} = \Gamma_i - \Gamma_{d_i} - \Gamma_{a_i}$, the AWC dynamics (37) and (38), and the error dynamics (42). It can be deduced that

$$\|w - w_d\| \leq \sqrt{2\gamma_w^2 \|d_w\|^2 + 2\gamma_a^2 \left\| \mathrm{Dz}^{\overline{T}}_{\underline{T}}(T) \right\|^2}, \tag{52}$$

$$\|\Gamma_i - \Gamma_{d_i}\| \leq \sqrt{2\gamma_{\Gamma_i}^2 \|d_{\Gamma_i}\|^2 + 2\gamma_{A_i}^2 \left\| \mathrm{Dz}^{\overline{\tau}_i}_{\underline{\tau}_i}(\tau_i) \right\|^2}. \tag{53}$$

Proof of Corollary 4: From Lemma 1, and letting $r = w, r_d = w_d, r_e = w_e$, and $r_a = w_a$ in (30) yields

$$\|w - w_d\| \leq \sqrt{2\|w_e\|^2 + 2\|w_a\|^2}. \tag{54}$$

Inserting (43) and (45) into (54), yields (52).

In a similar way, considering $r = \Gamma_i, r_d = \Gamma_{d_i}, r_e = \Gamma_{e_i}$, and $r_a = \Gamma_{a_i}$ in (30) leads to

$$\|\Gamma_i - \Gamma_{d_i}\| \leq \sqrt{2\|\Gamma_{e_i}\|^2 + 2\|\Gamma_{a_i}\|^2}. \tag{55}$$

Substituting (44) and (46) into (55) results in (53). ∎

Remark 3: It is evident from (52) and (53) that the upper bounds of $\|w - w_d\|$ and $\|\Gamma_i - \Gamma_{d_i}\|$ are related to the performance indices $(\gamma_w, \gamma_{\Gamma_i}, \gamma_a, \gamma_{A_i})$. Therefore, the following steps are performed to design the controller and AWC gains:

1) Set the desired performance indices: $\gamma_w, \gamma_{\Gamma_i}, \gamma_a, \gamma_{A_i}$.
2) From (28), obtain k_w, K_{Γ_i}, k_a, and K_{a_i} to achieve the favorable performance as follows:

$$\begin{aligned} &k_w \geq 1 + 1/\left(4\gamma_w^2\right), \ k_{\Gamma_i} \geq 1 + 1/\left(4\gamma_{\Gamma_i}^2\right), \\ &k_a \geq 1 + 1/\left(4\gamma_a^2\right), \ K_{a_i} \geq 1 + 1/\left(4\gamma_{A_i}^2\right). \end{aligned} \tag{56}$$

Remark 4: In this section, it was proved that $w_a \to 0$ and $\Gamma_{a_i} \to 0$, leading to $w_e \to w - w_d$ and $\Gamma_{e_i} \to \Gamma_i - \Gamma_{d_i}$. Consequently, the dynamics (42) converge to

$$\begin{aligned} m(\dot{w} - \dot{w}_d) &= -k_w(w - w_d) + d_w, \\ J_i(\dot{\Gamma} - \dot{\Gamma}_{d_i}) &= -K_{\Gamma_i}(\Gamma - \Gamma_{d_i}) + d_{\Gamma_i}, \end{aligned} \tag{57}$$

which are the nominal error dynamics. Therefore, it can be concluded that the performance of the AWC dynamics plays a key role in the convergence of the dynamics (42) to the nominal behavior, which can be directly influenced by the AWC gains. More precisely, defining $\tilde{u}_T = \mathrm{Dz}^{\overline{T}}_{\underline{T}}(T)$ and $\tilde{u}_{\tau_i} = \mathrm{Dz}^{\overline{\tau}_i}_{\underline{\tau}_i}(\tau_i)$, the AWC transfer functions are

$$\frac{w_a(\bar{s})}{\tilde{u}_T(\bar{s})} = \frac{1}{m\bar{s} + k_a}, \ \frac{\Gamma_{a_i}(s_i)}{\tilde{u}_{\tau_i}(s_i)} = -\frac{1}{J_i s_i + K_{a_i}}, \tag{58}$$

from which the poles of the AWC dynamics are $\bar{s} = -k_a/m$ and $s_i = -K_{a_i}/J_i$. As can be seen, the poles are directly related to the AWC gains, as shown in Step 2 of Remark 3.

B. Desired Signals for Tracking Problem

For a quadrotor, the x and y positions cannot be directly controlled by the control inputs [26], [27], [28]. Instead, these positions are indirectly controlled through the roll and pitch angles of the quadrotor [29]. By appropriately controlling the desired roll (ϕ_r) and pitch (θ_r) angles, the quadrotor can be maneuvered to the desired x and y positions (x_r and y_r) by defining the desired signals w_d and Γ_d as

$$w_d = w_r - k_z e_z, \tag{59}$$

$$\Gamma_d = \Gamma_r - K_\Theta e_\Theta. \tag{60}$$

where $e_z = z - z_r, w_r = \dot{z}_r, e_\Theta = [e_\phi, e_\theta, e_\psi]', e_\phi = \phi - \phi_r, e_\theta = \theta - \theta_r, e_\psi = \psi - \psi_r, \Gamma_r = [\dot{\phi}_r, \dot{\theta}_r, \dot{\psi}_r]'$, and $k_z, K_\Theta = \mathrm{diag}\{k_\phi, k_\theta, k_\psi\}$ are the positive gains. Since it was proved that $w \to w_d$ and $\Gamma \to \Gamma_d$, it follows from (59) and (60) that

$$\begin{aligned} &\dot{e}_z \to -k_z e_z \Rightarrow z \to z_r, \quad \dot{e}_\phi \to -k_\phi e_\phi \Rightarrow \phi \to \phi_r, \\ &\dot{e}_\theta \to -k_\theta e_\theta \Rightarrow \theta \to \theta_r, \quad \dot{e}_\psi \to -k_\psi e_\psi \Rightarrow \psi \to \psi_r. \end{aligned} \tag{61}$$

Moreover, in the absence of saturation and disturbance, the roll and pitch angles can be obtained from (3) – (5):

$$\begin{aligned} \theta &= \tan^{-1}\left((\ddot{x}\mathrm{c}_\psi + \ddot{y}\mathrm{s}_\psi)/\chi\right), \\ \phi &= \tan^{-1}\left((\ddot{x}\mathrm{s}_\psi \mathrm{c}_\theta - \ddot{y}\mathrm{c}_\psi \mathrm{c}_\theta)/\chi\right) \end{aligned} \tag{62}$$

where $\chi = \ddot{z} - g$. Defining the desired roll and pitch angles:

$$\begin{aligned} \theta_r &= \tan^{-1}\left((\zeta_1 \mathrm{c}_{\psi_r} + \zeta_2 \mathrm{s}_{\psi_r})/\chi_r\right), \\ \phi_r &= \tan^{-1}\left((\zeta_1 \mathrm{s}_{\psi_r} \mathrm{c}_{\theta_r} - \zeta_2 \mathrm{c}_{\psi_r} \mathrm{c}_{\theta_r})/\chi_r\right), \end{aligned} \tag{63}$$

where $\chi_r = \ddot{z}_r - g$, $\zeta_1 = \ddot{x}_r - k_u \dot{e}_x - k_x e_x$, $\zeta_2 = \ddot{y}_r - k_v \dot{e}_y - k_y e_y$, in which $e_x = x - x_r$ and $e_y = y - y_r$ are the tracking errors, k_x, k_y, k_u, and k_v are the positive gains. From (61), (62), and (63), it can be concluded that $\ddot{e}_x \to -k_u \dot{e}_x - k_x e_x \Rightarrow x \to x_r$, $\ddot{e}_y \to -k_v \dot{e}_y - k_y e_y \Rightarrow y \to y_r$. A schematic of the proposed method is illustrated in Fig. 1.

V. Simulation Results

In this section, the effectiveness of the proposed method is evaluated through simulation of the following scenarios, which consider the presence (or absence) of saturation on the vehicle's propeller speeds and the use (or absence) of AWC: 1) without saturation (nominal case); 2) with saturation, without AWC; 3) with saturation, with the proposed AWC, 4) with saturation, with an AWC design described in [15]. The last scenario is considered for comparison of an existing method that does not take disturbance into consideration, to

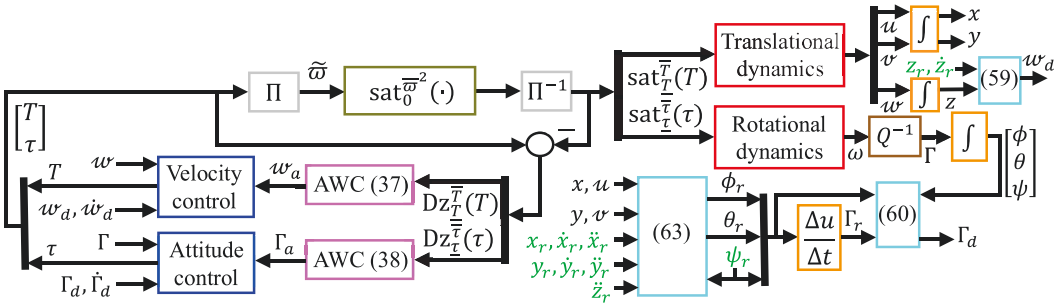

Fig. 1. Schematic of the proposed method.

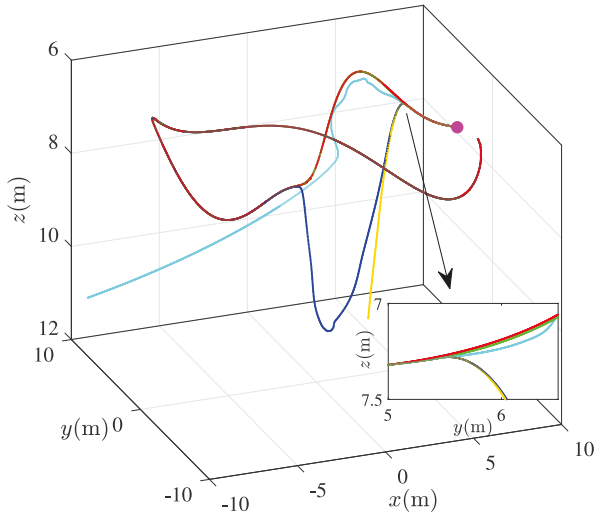

Fig. 2. Quadrotor trajectories. Initial position ●, Desired trajectory —, Without saturation —, With saturation, without AWC —, With saturation, with proposed AWC —, With saturation, with AWC method from [15] —.

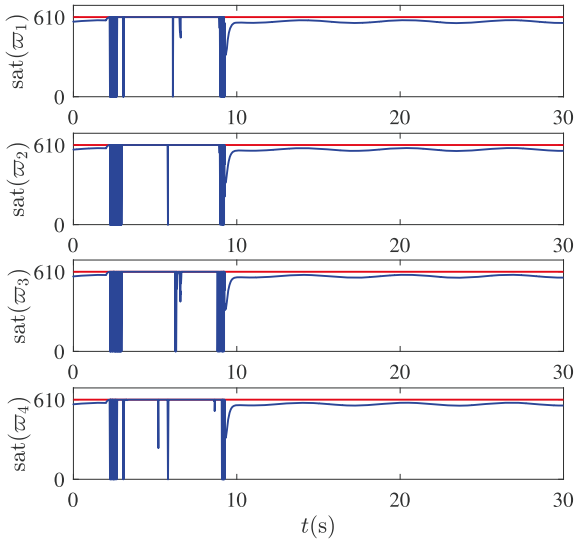

Fig. 3. Propeller speeds (rad/s).

illustrate the effectiveness of the proposed method, which includes disturbance in the design.

The quadrotor parameters are taken from [30]. The desired trajectory is chosen as [31]: $x_r = 8\cos(0.2t)$, $y_r = 7\sin(0.4t)$, $z_r = 0.35\sin(t) + 7$, where the desired yaw is $\psi_r = 0\ \forall t$. For the scenarios when saturation is present, the maximum propeller speed is $\overline{\varpi} = 610$ rad/s. The gains for the tracking problem are $k_x = k_y = k_z = k_u = k_v = 7$ and $K_\Theta = \text{diag}\{7, 7, 7\}$. The external wind disturbance is a rectangular signal active over the interval [2s, 3s] and applied in the $+z$-direction with a magnitude of 28.8% of the maximum thrust generated by a single propeller (i.e., $0.288k\overline{\varpi}^2$). The initial position of the quadrotor is at the starting point of the desired trajectory: $x(0) = 8, y(0) = 0$, and $z(0) = 7$ and the initial velocity is zero.

Using Corollaries 2 and 3, we aim to satisfy the following:

$$\|w_e\|/\|d_w\| \le \gamma_w, \quad \|w_a\|/\left\|\text{Dz}_{\underline{T}}^{\overline{T}}(T)\right\| \le \gamma_a, \tag{64}$$

$$\|\Gamma_{e_i}\|/\|d_{\Gamma_i}\| \le \gamma_{\Gamma_i}, \quad \|\Gamma_{a_i}\|/\left\|\text{Dz}_{\underline{\tau}_i}^{\overline{\tau}_i}(\tau_i)\right\| \le \gamma_{A_i}, \tag{65}$$

where $\gamma_w = \gamma_{\Gamma_i} = 0.2$, $\gamma_a = \gamma_{A_i} = 0.125$. From the second step of Remark 3: $k_w \ge 7.25$, $k_{\Gamma_i} \ge 7.25$, $k_a \ge 17$, $K_{a_i} \ge 17$. Therefore, we choose $k_w = K_{\Gamma_i} = 8$, $k_a = K_{a_i} = 17$.

In [15], deviation from nominal linear behavior in response to saturation is represented by a nonlinear mapping. A small $\mathcal{L}_2$ norm of this mapping indicates that the AWC effectively maintains performance close to the desired nominal behavior. To compare the results with the method in [15], the nominal control gains $(k_x, k_y, k_z, k_u, k_v, K_\Theta)$ remain unchanged, and the AWC gains are obtained by solving a set of linear matrix inequalities presented in Theorem 4 of that work. Implementing a narrowed sector bound on the deadzone with $\mathcal{A} = 0.64$, a lower bound of 0.33 for the $\mathcal{L}_2$ norm of the nonlinear mapping resulted from an optimization to minimize this bound. The corresponding AWC gain from this optimization is $F = \text{diag}(865.67, -5.65, -5.3981, -6.46)$.

The quadrotor trajectories for the four scenarios are plotted in Fig. 2. Without actuator saturation, the quadrotor tracks the desired trajectory despite the wind disturbance. Of course for this scenario, no limit exists on the amount of propeller thrust that can be produced. In the presence of saturation, when AWC is not used, the flight immediately deviates from the desired trajectory when the wind disturbance is applied and does not recover. However, with the use of proposed AWC, although there is a significant deviation from the desired trajectory during the wind disturbance, the quadrotor recovers and tracks the remaining portion of the desired trajectory. This is not the case for the method from [15]. Although the method provides a trajectory close to the desired trajectory during the period of the wind disturbance, it is unable to remain on the trajectory.

The propeller speeds for scenario 3): with saturation, with the proposed AWC, are presented in Fig. 3. The figure shows that while the propeller speeds are initially saturated, they eventually remain within the saturation limits after ≈ 7.5s.

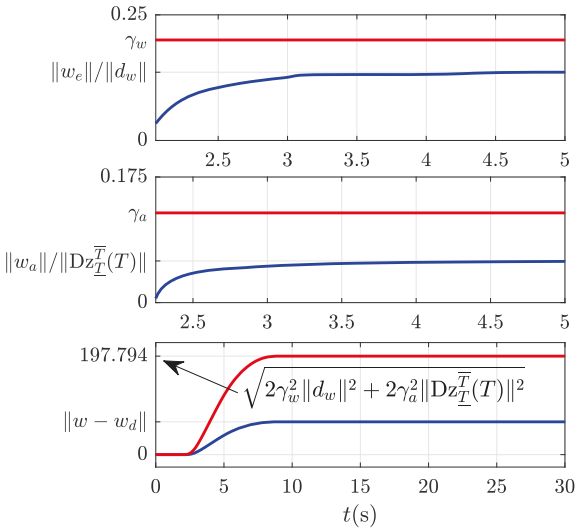

Fig. 4. Performance curves: performance ▬, bound ▬.

The blue curves in the top two graphs of Fig. 4 illustrate $\sqrt{\int_0^t w_e^2\,\mathrm{d}t}/\sqrt{\int_0^t d_w^2\,\mathrm{d}t}$ and $\sqrt{\int_0^t w_a^2\,\mathrm{d}t}/\sqrt{\int_0^t \mathrm{Dz}_{\underline{T}}^{\overline{T}}(T)^2\mathrm{d}t}$, calculated from the simulation data. It is evident from these graphs that conditions (64) are satisfied. Also, the blue and red curves in the bottom graph show $\sqrt{\int_0^t (w-w_d)^2\,\mathrm{d}t}$ and $\sqrt{2\gamma_w^2\int_0^t d_w^2\mathrm{d}t+2\gamma_a^2\int_0^t \mathrm{Dz}_{\underline{T}}^{\overline{T}}(T)^2\mathrm{d}t}$ calculated from the simulation data, indicating that (52) from Corollary 4 is satisfied.

VI. Conclusion

This letter addresses the trajectory tracking control problem for quadrotors with constrained propeller speeds and operating in the presence of external wind disturbances. An AWC is introduced to address the effects of propeller speed saturation. In addition, to achieve the desired tracking error performance, theoretical upper bounds are derived, which depend on the controller and AWC gains. Therefore, the desired performance is ensured through the choice of these gains. Simulation results are presented to demonstrate the effectiveness and validity of the proposed control method.

References

[1] Y. Song, L. He, D. Zhang, J. Qian, and J. Fu, "Neuroadaptive fault-tolerant control of quadrotor UAVs: A more affordable solution," *IEEE Trans. Neural Netw. Learn. Syst.*, vol. 30, no. 7, pp. 1975–1983, Jul. 2019.

[2] S. Xie, Q. Chen, and X. He, "Predefined-time approximation-free attitude constraint control of rigid spacecraft," *IEEE Trans. Aerosp. Electron. Syst.*, vol. 59, no. 1, pp. 347–358, Feb. 2023.

[3] M. Tao, Q. Chen, X. He, and S. Xie, "Fixed-time filtered adaptive parameter estimation and attitude control for quadrotor UAVs," *IEEE Trans. Aerosp. Electron. Syst.*, vol. 58, no. 5, pp. 4135–4146, Oct. 2022.

[4] S. Zhao, Y. Xia, L. Ma, and H. Yang, "Finite-time height control of quadrotor UAVs," *Appl. Sci.*, vol. 13, no. 13, p. 7914, 2023.

[5] M. Rinaldi, S. Primatesta, and G. Guglieri, "A comparative study for control of quadrotor UAVs," *Appl. Sci.*, vol. 13, no. 6, p. 3464, 2023.

[6] L. Zhao, L. Dai, Y. Xia, and P. Li, "Attitude control for quadrotors subjected to wind disturbances via active disturbance rejection control and integral sliding mode control," *Mech. Syst. Signal Process.*, vol. 129, pp. 531–545, Aug. 2019.

[7] K. Chen et al., "A novel open-closed-loop control strategy for quadrotor trajectory tracking on real-time control and acquisition platform," *Appl. Sci.*, vol. 13, no. 5, p. 3251, 2023.

[8] X. Zhang, B. Xian, B. Zhao, and Y. Zhang, "Autonomous flight control of a nano quadrotor helicopter in a GPS-denied environment using on-board vision," *IEEE Trans. Ind. Electron.*, vol. 62, no. 10, pp. 6392–6403, Oct. 2015.

[9] J. Zhao, H. Zhang, and X. Li, "Active disturbance rejection switching control of quadrotor based on robust differentiator," *Syst. Sci. Control Eng.*, vol. 8, no. 1, pp. 605–617, 2020.

[10] I. H. Imran, A. Can, R. Stolkin, and A. Montazeri, "Real-time nonlinear parameter estimation and tracking control of unmanned aerial vehicles in closed-loop," *Sci. Rep.*, vol. 13, no. 1, p. 3125, 2023.

[11] B. Dai, Y. He, G. Zhang, F. Gu, L. Yang, and W. Xu, "Wind disturbance rejection for unmanned aerial vehicle based on acceleration feedback method," in *Proc. IEEE Conf. Decision Control (CDC)*, 2018, pp. 4680–4686.

[12] B. Wang, Z. A. Ali, and D. Wang, "Controller for UAV to oppose different kinds of wind in the environment," *J. Control Sci. Eng.*, vol. 2020, no. 1, 2020, Art. no. 5708970.

[13] M. Shahbazzadeh, H. Salehifar, and S. J. Sadati, "Optimal dynamic output feedback control of Lipschitz nonlinear systems under input saturation," *J. Vib. Control*, vol. 29, nos. 1–2, pp. 158–168, 2023.

[14] M. Shahbazzadeh, H. Salehifar, and S. Jalil Sadati, "Observer-based control with enlarged domain of attraction for one-sided Lipschitz systems subject to input saturation," *Optimal Control Appl. Methods*, vol. 43, no. 2, pp. 495–511, 2022.

[15] M. C. Turner, G. Herrmann, and I. Postlethwaite, "Anti-windup compensation using a decoupling architecture," *Adv. Strategies Control Syst. Input Output Constraints*, pp. 121–171, 2007.

[16] E. Prempain, M. C. Turner, and I. Postlethwaite, "Coprime factor based anti-windup synthesis for parameter-dependent systems," *Syst. Control Lett.*, vol. 58, no. 12, pp. 810–817, 2009.

[17] W. Lai, Y. Li, and Z. Lin, "Performance-based activation of anti-windup compensation for control of linear systems subject to actuator saturation," *Automatica*, vol. 159, Jan. 2024, Art. no. 111298.

[18] M. C. Turner and C. M. Richards, "Constrained rigid body attitude stabilization: An anti-windup approach," *IEEE Control Syst. Lett.*, vol. 5, no. 5, pp. 1663–1668, Nov. 2021.

[19] G. Li, G. Herrmann, D. P. Stoten, J. Tu, and M. C. Turner, "A novel robust disturbance rejection anti-windup framework," *Int. J. Control*, vol. 84, no. 1, pp. 123–137, 2011.

[20] N. A. Ofodile and M. C. Turner, "Anti-windup design for input-coupled double integrator systems with application to quadrotor UAV's," *Eur. J. Control*, vol. 38, pp. 22–31, Nov. 2017.

[21] C. M. Richards and M. C. Turner, "Combined static and dynamic anti-windup compensation for quadcopters experiencing large disturbances," *J. Guid., Control, Dyn.*, vol. 43, no. 4, pp. 673–684, 2020.

[22] N. A. Ofodile, M. C. Turner, and O. C. Ubadike, "Channel-by-channel anti-windup design for a class of multivariable systems," in *Proc. Am. Control Conf. (ACC)*, 2015, pp. 2045–2050.

[23] N. A. Ofodile and M. C. Turner, "Decentralized approaches to anti-windup design with application to quadrotor unmanned aerial vehicles," *IEEE Trans. Control Syst. Technol.*, vol. 24, no. 6, pp. 1980–1992, Nov. 2016.

[24] B. E. Farber and C. M. Richards, "Adaptive control and parameter-dependent anti-windup compensation for inertia-varying quadcopters," *Int. J. Control*, vol. 97, no. 2, pp. 235–248, 2024.

[25] M. Shahbazzadeh and C. M. Richards, "Anti-windup compensator design for guidance and control of quadrotors," in *Proc. Am. Control Conf. (ACC)*, 2024, pp. 1695–1700.

[26] Y.-C. Liu and T.-W. Ou, "Non-linear adaptive tracking control for quadrotor aerial robots under uncertain dynamics," *Inst. Eng. Technol. Control Theory Appl.*, vol. 15, no. 8, pp. 1126–1139, 2021.

[27] S.-E.-I. Hasseni and L. Abdou, "Decentralized PID control by using GA optimization applied to a quadrotor," *J. Autom. Mobile Robot. Intell. Syst.*, vol. 12, no. 2, pp. 33–44, 2018.

[28] S. Berkane, A. Tayebi, and S. De Marco, "A nonlinear navigation observer using IMU and generic position information," *Automatica*, vol. 127, May 2021, Art. no. 109513.

[29] H. Elkholy and M. K. Habib, "Dynamic modeling and control techniques for a quadrotor," in *Unmanned Aerial Vehicles: Breakthroughs in Research and Practice*. Hershey, PA, USA: IGI Global, 2019, pp. 20–66.

[30] T. Kirven and J. B. Hoagg, "Autonomous quadrotor collision avoidance and destination seeking in a GPS-denied environment," *Auton. Robots*, vol. 45, pp. 99–118, Jan. 2021.

[31] R. J. Ruiz, J. L. Saravia, V. H. Andaluz, and J. S. Sánchez, "Virtual training system for unmanned aerial vehicle control teaching–learning processes," *Electronics*, vol. 11, no. 16, p. 2613, 2022.